Inorganic Chemistry

pubs.acs.org/IC Article

Structural Basis for the Effects of Phenylalanine on Tuning the Reduction Potential of Type 1 Copper in Azurin

Yiwei Liu, Nicholas M. Marshall, Sheng-Song Yu, Wantae Kim, Yi-Gui Gao, Howard Robinson, Mark J. Nilges, Yan Zhang, Siu Yee New,* and Yi Lu*

Cite This: *Inorg. Chem.* 2023, 62, 11618−11625 Read Online

ACCESS | Metrics & More | Article Recommendations | Supporting Information

ABSTRACT: In order to investigate the effects of the secondary coordination sphere in fine-tuning redox potentials ($E^{\circ\prime}$) of type 1 blue copper (T1Cu) in cupredoxins, we have introduced M13F, M44F, and G116F mutations both individually and in combination in the secondary coordination sphere of the T1Cu center of azurin (Az) from *Pseudomonas aeruginosa*. These variants were found to differentially influence the $E^{\circ\prime}$ of T1Cu, with M13F Az decreasing $E^{\circ\prime}$, M44F Az increasing $E^{\circ\prime}$, and G116F Az showing a negligible effect. In addition, combining the M13F and M44F mutations increases $E^{\circ\prime}$ by 26 mV relative to WT-Az, which is very close to the combined effect of $E^{\circ\prime}$ by each mutation. Furthermore, combining G116F with either M13F or M44F mutation resulted in negative and positive cooperative effects, respectively. Crystal structures of M13F/M44F-Az, M13F/G116F-Az, and M44F/G116F-Az combined with that of G116F-Az reveal these changes arise from steric effects and fine-tuning of hydrogen bond networks around the copper-binding His117 residue. The insights gained from this study would provide another step toward the development of redox-active proteins with tunable redox properties for many biological and biotechnological applications.

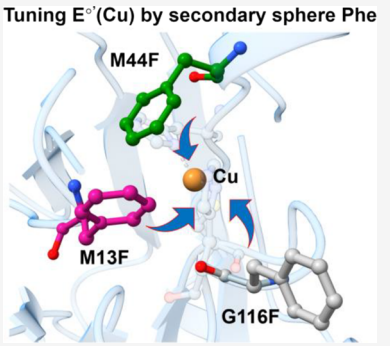

INTRODUCTION

Type 1 copper (T1Cu) proteins are a widely studied class of electron transfer (ET) proteins with reduction potentials ($E^{\circ\prime}$) spanning a range of >500 mV. The ability of T1Cu proteins to attain a wide range of potentials is one of the reasons they are ubiquitously found as ET centers in critical biological processes, including respiration, photosynthesis, and biomass conversion.[1−8] Because T1Cu centers are exceptionally efficient at ET, they have been proposed to serve as electron carriers in bio-inspired devices, such as fuel cells.[9−13]

Despite exhibiting a wide range of $E^{\circ\prime}$, all T1Cu proteins utilize an almost identical primary coordination sphere (PCS) consisting of the thiol sidechain of one cysteine (Cys) and the imidazole sidechain of two histidine (His) residues in a distorted trigonal planar (Figure 1A) geometry.[14−16] Mutations to any ligand within the conserved PCS not only alter the spectroscopic characteristics of the T1Cu site but also lower the ET rate and efficiency.[17−19] These results suggest that in order for T1Cu proteins to possess such a wide range of $E^{\circ\prime}$ without affecting ET efficiency, noncovalent interactions in the secondary coordination sphere (SCS) of the T1Cu site—such as hydrophobicity, hydrogen bonding interactions, and dipole effects—must play an important role.[6,8] Therefore, a major focus in the current field of ET proteins is to elucidate the effects of these noncovalent interactions on $E^{\circ\prime}$. Success in this endeavor will not only result in a deeper understanding of bio-coordination chemistry and ET properties but also aid in tailoring highly efficient redox agents for practical applications,

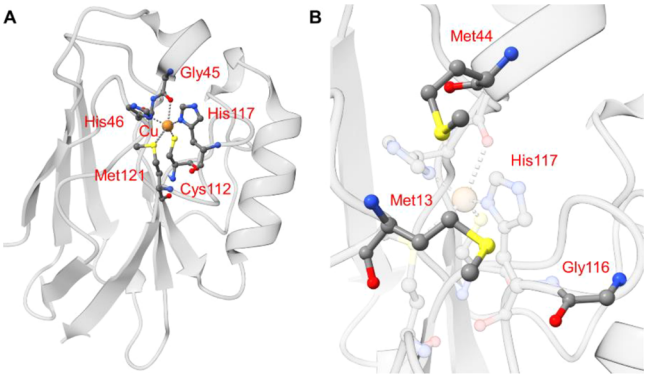

Figure 1. T1Cu center in Az from *Pseudomonas aeruginosa* (PDB: 4AZU).[1] (A) PCS of the T1Cu consisting of Gly45, His46, Cys112, His117, and the weakly-bound Met121 coordinated to T1Cu; (B) Met13, Met44, and Gly116 located in the SCS as candidate residues for their mutations to Phe to tune the hydrophobicity in the SCS and thus $E^{\circ\prime}$ of T1Cu.

Received: April 26, 2023
Published: July 10, 2023

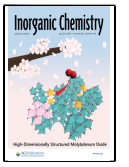

https://doi.org/10.1021/acs.inorgchem.3c01365
Inorg. Chem. 2023, 62, 11618−11625

ranging from biophysical studies of redox processes to alternative energy systems.

In comparison to studying PCS effects, probing the SCS is often more challenging, as the latter typically induces more subtle electronic and structural perturbations and thus requires more careful experimental design and detailed characterization. Toward this goal, several studies have contributed to the advance of this field that include not only T1Cu proteins[20−28] but also other redox-active proteins such as those containing purple Cu_A center,[29−32] iron and manganese superoxide dismutase,[33−36] the heme-Cu_B active site cytochrome *c* oxidase[37,38] and Fe-S proteins.[6,39−42] In previous publications, we have shown that $E^{\circ\prime}$ of T1Cu azurin (Az) can be fine-tuned across a wide range of $E^{\circ\prime}$ under physiological conditions, i.e., from −1 to +1 V vs standard hydrogen electrode (SHE) (all $E^{\circ\prime}$ stated hereafter are vs SHE) by altering the hydrophobicity, hydrogen bond interactions, and the coordinated metals (Cu vs Ni) in the SCS of the T1Cu center.[21,43] The introduction of phenylalanine (Phe) to the SCS has been critical in accomplishing this tuning, as it allows the hydrophobicity of the T1Cu to be modulated. For example, the introduction of M44F and G116F to the N47S/F114N/M121L-Az variant resulted in an increase of $E^{\circ\prime}$ from ∼690 to 970 ± 20 mV at pH 5.0, the highest $E^{\circ\prime}$ of any engineered copper protein to date.[21,43] Despite these successes, the structural basis for such hydrophobicity-based redox tuning using Phe has not been elucidated.

Herein, we report a systematic study of M13F, M44F, and G116F mutations in Az, both individually and in several combinations (Figure 1). Through a combination of UV−vis absorption and electron paramagnetic resonance (EPR) spectroscopies together with electrochemical and X-ray crystallographic characterization, we have investigated the effects of these mutations on the redox and electronic properties of Az. As a result, we have found that the introduction of Phe at different SCS locations and in varying combinations with other mutations can modulate $E^{\circ\prime}$ in significantly different ways. X-ray crystal structures of these mutants reveal different spatial orientations of both Phe residues and hydrogen bond networks around the T1Cu-coordinating His117, which are responsible for such effects. Together, our findings suggest that the exact positioning of the introduced Phe is critical to successfully tuning $E^{\circ\prime}$ of the T1Cu center.

EXPERIMENTAL SECTION

Expression of Az Variants. Az mutants were constructed, expressed, and purified in the apo form (i.e., no Cu added) using a previously reported procedure.[44] All variants were further purified by size-exclusion chromatography, and only the monomer fractions were selected for other experiments. Holoprotein was obtained by stepwise titration of 5 mM $CuSO_4$ (1 μL each) into apoprotein and monitored by UV−vis spectroscopy. Titration was continued until ∼Abs_{620} was constant with further copper addition. The holoprotein was then concentrated in Milipore-Amicon Centrifugal Filter (10,000 Da cutoff), washed with 50 mM NH_4OAc buffer at pH 6.35, and passed through a disposable prepacked PD-10 column (Cytiva, USA) to remove excess Cu^{2+}.

Spectroscopic Studies of Az Variants. Mass spectra were recorded on a Macromass Quattro II Mass Spectrometer using nondenaturing solvent (50 mM NH_4OAc, pH 6.35) at 50 °C, cone voltage of 30 V, capillary voltage of 2.4 V. The obtained spectra were processed by the Waters MassLynx data system. UV−visible absorption spectra were recorded on a Varian Cary 3E UV−visible spectrophotometer at ambient temperature and pH 6.35. EPR samples were prepared as frozen glass in a mixed buffer containing 50 mM NH_4OAc, 40 mM MOPS, 40 mM MES, 40 mM Tris, 40 mM CAPS, and 100 mM NaCl at pH 7:glycerol (1:1) and measured with a Varian E-line 12″ Century Series X-Band CW spectrometer at frequency 9.04 GHz; power 0.2−2.0 mW; modulation amplitude 4 G; temperature 60 K.

The instrument was equipped with an APD Helium cryostat and was maintained by the Illinois EPR Research Center (IERC). Simulation of EPR spectra was performed using the Simpow6 software package to determine g and $A_{\parallel}$ values.[45,46] Extinction coefficients were calculated based on the absolute amount of Cu in protein samples measured by inductively coupled plasma-mass spectrometry (ICP-MS) (performed at the Jackson School of Geosciences at the University of Texas at Austin).

Electrochemical Measurement. Cyclic voltammetry (CV) was performed on a CH Instrument model 620A Electrochemical Analyzer (Austin, Texas), using a mixed buffer containing 50 mM NH_4OAc, 40 mM MOPS, 40 mM MES, 40 mM Tris, 40 mM CAPS, and 100 mM NaCl (ranged from pH 4 to 9). All the buffer solutions were degassed by bubbling with nitrogen prior to data collection. Pyrolytic graphite edge (PGE) working electrodes were assembled by a previously published procedure.[47] A platinum wire auxiliary electrode and Ag/AgCl reference electrode (Bioanalytical Systems, West Lafayette, 1 N, 3 M NaCl) were also connected to the potentiostat. The Ag/AgCl reference electrode was calibrated against a standard calomel electrode (SCE) ($E^{\circ\prime}$ = 0.253 V at 4 °C). The PGE electrode was then polished with 0.05 μm alumina on a nylon polishing pad, followed by sonication in deionized water to remove excess alumina. The protein solution, typically 2 μL of 2−4 mM protein, was then applied to the graphite surface. 3−4 min of incubation at 4 °C was sufficient to absorb enough protein. The electrode was then immersed in the cold, degassed electrolyte solution for 2 min to equilibrate and then scanned for redox potential. Voltammograms were collected at a scan rate of 0.1 V/s, and no scan rate dependence of the peak positions was observed for all samples. Three measurements were performed on the same batch of each mutant using at least three different PGE electrodes. The average is reported as $E^{\circ\prime}$ in Table 1. All reported readings were converted to normal hydrogen electrode (NHE) potentials by adding 210 mV to the value obtained vs the Ag/AgCl reference.

Table 1. $E^{\circ\prime}$ of the T1Cu Center in WT-Az and Its Variants Containing Phe Mutations at pH 7.0 Midpoint potentials are reported vs SHE.

variants	$E^{\circ\prime}$ (mV)	$\Delta E^{\circ\prime}$ (mV)
WT-Az	278 ± 3	
M13F-Az	256 ± 8	−22
M44F-Az	325 ± 3	47
G116F-Az	282 ± 3	4
M13F/M44F-Az	304 ± 4	26
M13F/G116F-Az	242 ± 4	−36
M44F/G116F-Az	342 ± 3	64

Protein Crystallization and Optimization. Az variants were crystallized using vapor diffusion with hanging drop format. Variants are concentrated to 3 mM in a buffer of 50 mM NH_4OAc at pH 6.35. Crystals of M44F/G116F Az were obtained by mixing the protein sample with an equal volume of reservoir solutions consisting of 80 mM NaOAc-HOAc at pH 6.0, 0.29 M $CaCl_2$, 0.25 M $LiNO_3$, and 20% polyethylene glycol (PEG) 10,000. Blue crystals used later for X-ray diffraction studies were obtained after 1 week at 4 °C. Crystal of M13F/M44F Az was obtained under crystallization condition containing 0.1 M Tris−HCl at pH 8.0, 20 mM $CaCl_2$, 0.1 M $LiNO_3$, and 20% PEG 4000. The crystal was harvested after 6 months at room temperature. Crystals of both G116F Az and M13F/G116F Az were obtained using the protein sample at 1.5 mM in the crystallization condition containing 100 mM Tris−HCl at pH 8.0, 100

https://doi.org/10.1021/acs.inorgchem.3c01365
Inorg. Chem. 2023, 62, 11618−11625

mM $LiNO_3$,10 mM $CuSO_4$, and 20% PEG4000, using a volume ratio of 3:1 for protein sample over mother liquor at 4 °C. Plate-shape blue crystals appeared after 3−7 days. Despite repeated trials, we were unable to obtain the crystals for M13F Az and M44F Az.

Structure Determination and Refinement. X-ray diffraction data were acquired at the beamline 5.0.2 at the Advanced Light Source (ALS) of the Lawrence Berkeley National Laboratory or beamline 23-ID-B at the Advanced Photon Source (APS) of the Argonne National Laboratory. Diffraction images were processed and reduced with Xia2-DIALS[48,49] and AIMLESS[50] in the CCP4 software suite.[51,52] Molecular replacement solution was identified using wildtype Az protein (PDB: 4AZU) as the initial searching model using Phaser in the Phenix software suite.[53] The model building and refinement were performed in the Phenix.refine-WinCoot interface.[54,55] The final models were evaluated using Molprobity and ProCheck.[56,57] All structures were visualized and presented by the ChimeraX software suite.[58] The statistics for data collection and structure refinement are presented in Table S4.

RESULTS AND DISCUSSION

Spectroscopic Studies of Az Variants. The purity of the azurin mutants was confirmed by electrospray ionization mass spectrometry (ESI-MS) before spectroscopic characterization, which shows that the mass of all variants matches the calculated mass and within the experimental errors (±5 Da) (Figure S1). The addition of Cu^{2+} into the purified Az resulted in intense blue color for all variants studied. The UV−vis absorption spectra of these Az variants show a strong absorption band around 625 nm (ε = 2340−5835 M^{-1} cm^{-1}) (Figure 2A), consistent with the $S_{Cys}(p_\pi) \rightarrow Cu^{2+}(3d_{x2-y2})$ ligand-to-metal charge transfer (LMCT) band observed in WT-Az.[2,59−61] The X-band EPR spectra of these variants also appear very similar to WT-Az, exhibiting similar values for $g_{\|}$ and $A_{\|}$ (Figure 2B, Table S1). Taken together, the UV−vis and EPR spectroscopic data of the variants containing Phe mutations show that these mutations did not perturb the characters of the T1Cu center. The difference in the absorption intensity of the 625 nm band by different mutants at the same concentration, as shown in Figure 2A, is possibly caused by partial Zn incorporation at the T1Cu site, which commonly occurs during the recombinant expression of azurin in *Escherichia coli*.[62] To verify this hypothesis, we carried out ICP-MS experiments. Cu and Zn were detected and quantified in the Cu-reconstituted form of all variants (Table S2). The extinction coefficients calculated from the actual Cu concentrations are similar (5300−6367 M^{-1} cm^{-1}), which is consistent with the similar absorption wavelength and EPR pattern observed among all mutants.

Electrochemical Studies. All variants exhibit reversible one-electron redox processes as evidenced by CV, suggesting the structural integrity is maintained on the electrode (Figure S2). The resulting $E^{\circ\prime}$ for all variants investigated in this study is listed in Table 1. The observed $E^{\circ\prime}$ for WT-Az (278 ± 3 mV at pH 7.0) is consistent with the published values measured by redox titration and CV with both free and immobilized proteins.[21,63] Substitution of single Phe at positions 13, 44, and 116 have different effects on $E^{\circ\prime}$: M13F-Az decreases $E^{\circ\prime}$ by 22 mV relative to WT-Az; M44F-Az raises $E^{\circ\prime}$ by 47 mV; G116F-Az has a minimal effect on $E^{\circ\prime}$, increasing by only 4 mV (slightly above the standard deviation of ±3 mV). These data suggest that the incorporation of Phe produces substantially different effects on $E^{\circ\prime}$ of the T1Cu center depending on the precise spatial location.

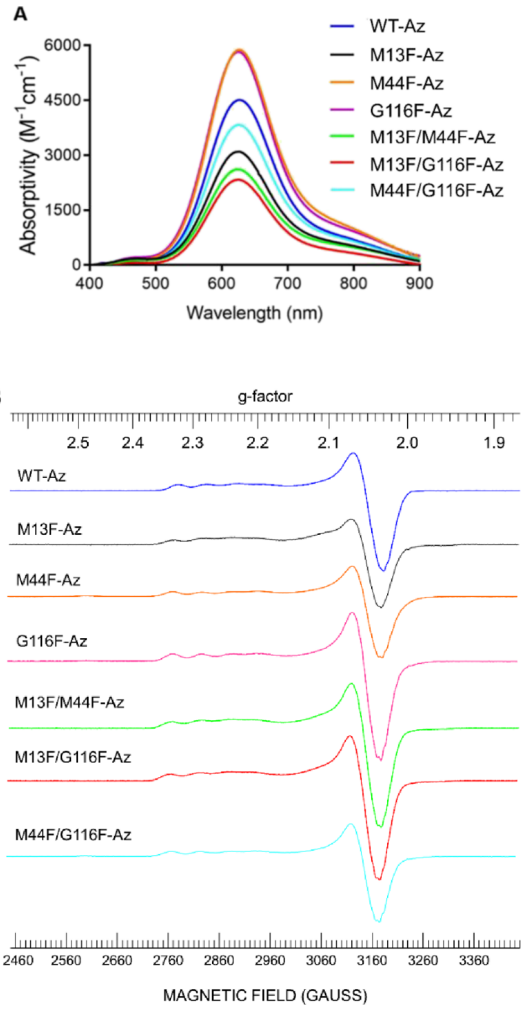

Figure 2. UV−vis (A) and X-band EPR (B) spectra of WT-Az and the Az variants.

Interestingly, the double mutant M13F/M44F-Az increases $E^{\circ\prime}$ by 26 mV relative to WT-Az, which is very close to the combined effect of $E^{\circ\prime}$ by each mutation (i.e., −22 mV from M13F-Az and + 47 mV from M44F-Az) suggesting an additive effect between these two mutations. In contrast, although the G116F mutation alone has a minimal effect on the $E^{\circ\prime}$, introducing the G116F mutation into M13F-Az decreases $E^{\circ\prime}$ by 36 mV, 14 mV lower than the M13F mutation alone. Meanwhile, the introduction of the G116F mutation into M44F-Az increases $E^{\circ\prime}$ by 64 mV, a 17 mV greater increase than the M44F mutation alone. These data suggest that while some Phe mutations are additive, others are cooperative.

Structural Analysis of M13F/M44F-Az. To better understand the structural basis of the effects of M13F and M44F mutations on $E^{\circ\prime}$ of the T1Cu center, we have obtained an X-ray crystal structure of M13F/M44F-Az at 3.0 Å resolution. Both the overall scaffolds (Figure 3A) and the T1Cu PCS (Figure 3B) of M13F/M44F-Az are almost superimposable to those of WT-Az. The bond lengths between Cu and the PCS residues are summarized in Table S3. A distance parameter R is defined by the difference between the bond length of Cu-S(Cys) and the average of two Cu-N(His) to evaluate the PCS pattern (Table S3). The M13F/M44F-Az, as well as other variants, shows similar R values compared to WT-Az. The highly similar metal coordination sphere and the

https://doi.org/10.1021/acs.inorgchem.3c01365
Inorg. Chem. 2023, 62, 11618−11625

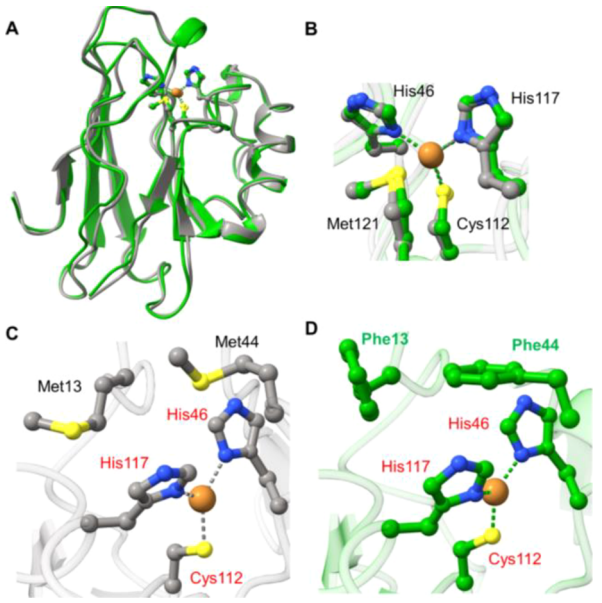

Figure 3. Superposition of M13F/M44F-Az (green) with WT-Az (gray; PDB: 4AZU) for (A) Az monomers and (B) at the T1Cu binding sites. (C and D) Residues at positions 13 and 44 and their hydrophobic encapsulation on His117 are highlighted in (C) WT-Az and (D) M13F/M44F-Az. Labels for Cu binding sites and unmutated residues are in red and black, respectively.

overall folding provide a structural explanation for the similarity of UV−vis and EPR spectra between M13F/M44F-Az and WT-Az. As shown in Figure 3C, Met13 in WT-Az is spatially close to His117, a T1Cu ligand with its imidazole ring partially exposed to solvent. The side chain of Met13 has evolved to closely pack next to His117, blocking the access of bulk solvent to His117. Even though Phe is more hydrophobic than Met and expected to increase $E^{\circ\prime}$ of the T1Cu center,[5,64,65] Phe13 does not fit into the groove normally filled by Met13. As a result of this steric constraint, the Phe ring adapts an orientation extending the phenyl ring into the solvent away from His117 (Figure 3D), making the area less hydrophobic than in WT-Az. This structural alteration caused by the mutation explains the unexpected decrease of $E^{\circ\prime}$ observed in M13F-Az.

In contrast, the side chain of residue 44 is less spatially restricted by the surrounding residues. The aromatic ring of Phe44 is oriented toward His117, increasing the hydrophobicity of the T1Cu site. As a result, Phe44 exerts a greater hydrophobic effect than Met44, and thus increases $E^{\circ\prime}$ as shown in Table 1. Additionally, although Met13 and Met44 are spatially close to one another, their mutations to Phe do not generate any steric clashes (Figure 3D). Therefore, the observed $E^{\circ\prime}$ of the M13F/M44F-Az double mutant is additive to the individual mutations.

Structural Analyses of G116F-Az, M13F/G116F-Az, and M44F/G116F-Az. Crystal structures of G116F Az and M13F/G116F Az were acquired at 2.2 and 1.5 Å resolution, respectively. An overlay of crystal structures of G116F Az and M13F/G116F Az with WT-Az are shown in Figure 4A,B. Among all three mutants, the M13F/G116F-Az shows the smallest structural deviation of the PCS compared to the WT, with the change of Cu-X bonds not greater than ±0.1 Å (Table S3). Both M44F/G116F-Az and G116F-Az have shortened Cu-O(Gly45) bonds by −0.3 and −0.5 Å, respectively, and lengthened Cu-N(His117) bonds by +0.2 and +0.2 Å. Similar levels of PCS changes have been observed in previous studies,

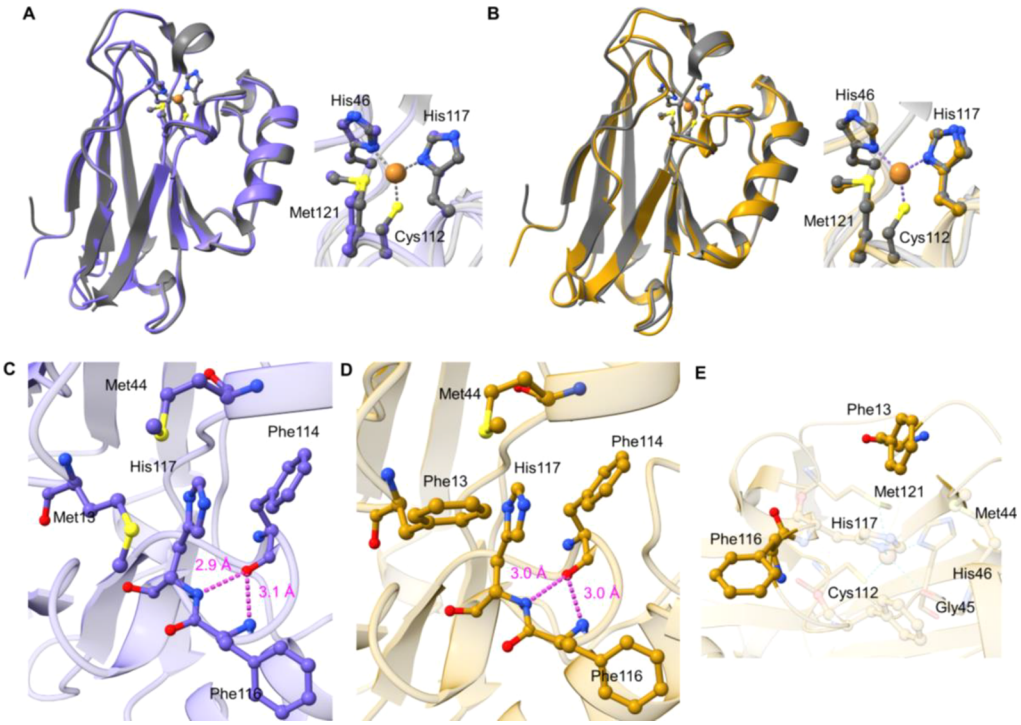

Figure 4. Crystal structure overlay of (A) G116F Az (purple, PDB 7U2F) and (B) M13F/G116F Az (gold, PDB 7TNC) with WT-Az (gray, PDB 4AZU). The PCS Cu coordination by His46, His117, and Cys112 are shown separately. The hydrogen bond triangle around Phe114 of (C) G116F-Az and (D) M13F/G116F Az is also shown. The two important hydrogen bond interactions (the "hydrogen bond triangle") are labeled in magenta to make a direct comparison between (C) and (D). Positions of the Phe13 and Phe116 residues in M13F/G116F are highlighted in (E).

https://doi.org/10.1021/acs.inorgchem.3c01365
Inorg. Chem. 2023, 62, 11618−11625

which nevertheless do not impose a certain consistent effect on $E^{\circ\prime}$[66−69] to a degree comparable to SCS tuning.[21,43]

The crystal structure of the single mutant G116F-Az shows that the Phe116 residue is solvent-exposed and points outward from the protein surface (Figure 4C). Similar orientations of Phe116 are also observed in the other two double mutants, M13F/G116F (Figure 4D) and M44F/G116F (Figure 5D). As a result, introducing Phe at the Gly116 position introduces minimal additional hydrophobic effect on the T1Cu site. This structural finding explains the negligible effect of the single Phe116 substitution on $E^{\circ\prime}$ compared to WT-Az (Table 1). This includes minimal perturbation of the hydrogen bonding network consisting of the interactions of the backbone atoms involving $O_{carbonyl}$(Phe114)/N_{amide}(Phe116), and $O_{carbonyl}$(Phe114)/N_{amide}(His117) (Figure 4C).

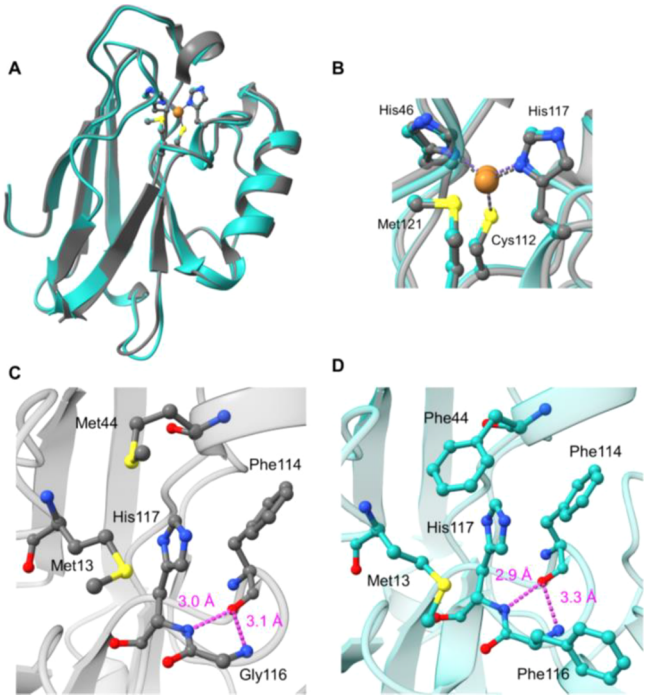

Figure 5. Superimposition of the overall structures (A) and PCS of T1Cu center (B) of M44F/G116F-Az (cyan) and WT-Az (gray; PDB: 4AZU). The effect of mutations at positions 44 and 116 on its surrounding residues before the mutation (C) (WT-Az) and after the mutation (D) (M44F/G116F-Az). Residue at position 44 and Phe114 affect the exposure of His117 to surrounding water. The two important hydrogen bond interactions (the "hydrogen bond triangle") are labeled in magenta.

As indicated by the experimental results, combining Phe116 with M13F or M44F shows negative and positive cooperative effects in tuning the T1Cu potential, respectively (Table 1). When M44F is combined with G116F, the aromatic rings of both Phe44 and Phe114 block His117 from the surrounding water, causing an increase in hydrophobicity and thus an increase in reduction potential relative to WT-Az (Figure 5D). On the other hand, when M13F is incorporated into the G116F variant, the orientation of Phe13 in M13F/G116F is perpendicular to the His117 residue (Figure 4E), which leaves a relatively open site for the solvent to access and thus lowers the $E^{\circ\prime}$. Importantly, the hydrogen bond between $O_{carbonyl}$(Phe114) and N_{amide}(Phe116) is lengthened by 0.2 Å in the M44F/G116F variant (Figure 5D) compared to the WT-Az (Figure 5C), and further by 0.3 Å compared to the M13F/G116F (Figure 4D) variant. In previous studies, we have demonstrated that Phe114 is an important residue in the SCS hydrogen bond network and the nonlocal electrostatic interactions that govern $E^{\circ\prime}$ of Cu.[21,43,70] The different conformations of Phe13 and Phe44 relative to His117 and the subtle change of the hydrogen bond between Phe114 and Phe116 may result in the inversed cooperative $E^{\circ\prime}$ tuning effect between M13F/G116F and M44F/G116F.

CONCLUSIONS

In the present study, we have shown that the introduction of phenylalanine residues around the T1Cu in Az (i.e., M13F, M44F, and G116F mutations) results in different, and sometimes opposite, effects on $E^{\circ\prime}$, wherein single mutations either increase, decrease, or have little effect on $E^{\circ\prime}$ depending on spatial positioning. Likewise, these effects can be either additive or cooperative when mutations are combined. Hence, simply introducing Phe in the vicinity of the T1Cu center is insufficient to induce a predictable increase based on increasing hydrophobicity, and both the location of the mutation and choice of single mutation combinations are important in determining the outcome on $E^{\circ\prime}$. The exact positioning of the mutations is important to controlling factors that can negate any hydrophobicity effects that should raise the $E^{\circ\prime}$, including steric conflicts, solvent exposure, and changes in hydrogen bonding. The insights gained from these detailed structural studies are critical toward understanding the molecular effects of such mutations, aiding in the rational design of metalloproteins with predictable $E^{\circ\prime}$ and functional properties associated with $E^{\circ\prime}$.

ASSOCIATED CONTENT

Supporting Information

The Supporting Information is available free of charge at https://pubs.acs.org/doi/10.1021/acs.inorgchem.3c01365.

Mass spectra, CV plots, ICP-MS result, and summary of crystallography data (PDF)

AUTHOR INFORMATION

Corresponding Authors

Yi Lu − *Department of Chemistry, McKetta Department of Chemical Engineering, and Interdisciplinary Life Sciences Graduate Programs, The University of Texas at Austin, Austin, Texas 78712, United States; Department of Chemistry, University of Illinois at Urbana-Champaign, Urbana, Illinois 61801, United States;* orcid.org/0000-0003-1221-6709; Email: yi.lu@utexas.edu

Siu Yee New − *School of Pharmacy, Faculty of Science and Engineering, University of Nottingham Malaysia, Semenyih, Selangor Darul Ehsan 43500, Malaysia;* orcid.org/0000-0003-4392-3852; Email: siuyee.new@nottingham.edu.my

Authors

Yiwei Liu − *Department of Chemistry, The University of Texas at Austin, Austin, Texas 78712, United States; Department of Chemistry, University of Illinois at Urbana-Champaign, Urbana, Illinois 61801, United States;* orcid.org/0000-0002-7899-2279

Nicholas M. Marshall − *Department of Chemistry, University of Illinois at Urbana-Champaign, Urbana, Illinois 61801, United States*

Sheng-Song Yu − *Department of Chemistry, University of Illinois at Urbana-Champaign, Urbana, Illinois 61801, United States; Department of Environmental Science and Engineering, University of Science and Technology of China, Hefei, Anhui 230026, P. R. China*

Wantae Kim − *McKetta Department of Chemical Engineering, The University of Texas at Austin, Austin, Texas 78712, United States*

Yi-Gui Gao − *Department of Chemistry, University of Illinois at Urbana-Champaign, Urbana, Illinois 61801, United States*

Howard Robinson − *Biology Department, Brookhaven National Laboratory, Upton, New York 11973, United States*

Mark J. Nilges − *Department of Chemistry, University of Illinois at Urbana-Champaign, Urbana, Illinois 61801, United States*

Yan Zhang − *Department of Molecular Biosciences, The University of Texas at Austin, Austin, Texas 78712, United States; Interdisciplinary Life Sciences Graduate Programs, The University of Texas at Austin, Austin, Texas 78712, United States;* orcid.org/0000-0002-9360-5388

Complete contact information is available at: https://pubs.acs.org/10.1021/acs.inorgchem.3c01365

Notes

The authors declare no competing financial interest.

■ ACKNOWLEDGMENTS

This work was supported by the National Science Foundation (CHE-2201279). We also thank the Robert A. Welch Foundation (Grant F-0020) for support of the Lu group research program at the University of Texas at Austin. Crystallographic data was acquired at the Advanced Light Source beamline 5.0.2 (proposal ALS-11565) of the Lawrence Berkeley National Laboratory, and the Advanced Photon Source beamline GM/CA 23-IDD (proposal 81327) of the Argonne National Laboratory. We thank Dr. Casey Van Stappen and Mr. Jingxiang Wang for proofreading this manuscript, Dr. Daniil Prigozhin at ALS and Dr. Craig Ogata at APS for their help in crystallography data collection, Dr. Zhenglin Yang and Dr. Nathaniel Miller for assisting in the ICP-MS experiments.

■ REFERENCES

(1) Choi, M.; Davidson, V. L. Cupredoxins—A Study of How Proteins May Evolve to Use Metals for Bioenergetic Processes. *Metallomics* **2011**, *3*, 140.

(2) Solomon, E. I.; Szilagyi, R. K.; DeBeer George, S.; Basumallick, L. Electronic Structures of Metal Sites in Proteins and Models: Contributions to Function in Blue Copper Proteins. *Chem. Rev.* **2004**, *104*, 419−458.

(3) Dennison, C. Investigating the Structure and Function of Cupredoxins. *Coord. Chem. Rev.* **2005**, *249*, 3025−3054.

(4) Gray, H. B.; Malmström, B. G.; Williams, R. J. P. Copper Coordination in Blue Proteins. *J. Biol. Inorg. Chem.* **2000**, *5*, 551−559.

(5) Hosseinzadeh, P.; Lu, Y. Design and Fine-Tuning Redox Potentials of Metalloproteins Involved in Electron Transfer in Bioenergetics. *Biochim. Biophys. Acta, Bioenerg.* **2016**, *1857*, 557−581.

(6) Liu, J.; Chakraborty, S.; Hosseinzadeh, P.; Yu, Y.; Tian, S.; Petrik, I.; Bhagi, A.; Lu, Y. Metalloproteins Containing Cytochrome, Iron−Sulfur, or Copper Redox Centers. *Chem. Rev.* **2014**, *114*, 4366−4469.

(7) Lu, Y. Electron Transfer: Cupredoxins. In *Biocoord. Chem.*; Que, J. L., Tolman, W. B., Meyer, T. J., Eds.; McCleverty, J. A., Series Ed.; Comprehensive Coordination Chemistry II: From Biology to Nanotechnology; Elsevier: Oxford, UK, 2004; Vol. *8*, p 91.

(8) Van Stappen, C.; Deng, Y.; Liu, Y.; Heidari, H.; Wang, J.-X.; Zhou, Y.; Ledray, A. P.; Lu, Y. Designing Artificial Metalloenzymes by Tuning of the Environment beyond the Primary Coordination Sphere. *Chem. Rev.* **2022**, *122*, 11974−12045.

(9) Chumillas, S.; Maestro, B.; Feliu, J. M.; Climent, V. Comprehensive Study of the Enzymatic Catalysis of the Electrochemical Oxygen Reduction Reaction (ORR) by Immobilized Copper Efflux Oxidase (CueO) from Escherichia Coli. *Front. Chem.* **2018**, *6*, 358.

(10) Hudson, J. M.; Heffron, K.; Kotlyar, V.; Sher, Y.; Maklashina, E.; Cecchini, G.; Armstrong, F. A. Electron Transfer and Catalytic Control by the Iron−Sulfur Clusters in a Respiratory Enzyme, *E. Coli* Fumarate Reductase. *J. Am. Chem. Soc.* **2005**, *127*, 6977−6989.

(11) Beratan, D. N.; Onuchic, J. N.; Winkler, J. R.; Gray, H. B. Electron-Tunneling Pathways in Proteins. *Science* **1992**, *258*, 1740−1741.

(12) Blanford, C. F.; Heath, R. S.; Armstrong, F. A. A Stable Electrode for High-Potential, Electrocatalytic O_2 Reduction Based on Rational Attachment of a Blue Copper Oxidase to a Graphite Surface. *Chem. Commun.* **2007**, 1710−1712.

(13) Kanan, M. W.; Nocera, D. G. In Situ Formation of an Oxygen-Evolving Catalyst in Neutral Water Containing Phosphate and Co^{2+}. *Science* **2008**, *321*, 1072−1075.

(14) Nar, H.; Messerschmidt, A.; Huber, R.; van de Kamp, M.; Canters, G. W. Crystal Structure Analysis of Oxidized Pseudomonas Aeruginosa Azurin at pH 5.5 and pH 9.0. A pH-Induced Conformational Transition Involves a Peptide Bond Flip. *J. Mol. Biol.* **1991**, *221*, 765−772.

(15) Nar, H.; Messerschmidt, A.; Huber, R.; van de Kamp, M.; Canters, G. W. Crystal Structure of Pseudomonas Aeruginosa Apo-Azurin at 1.85 A Resolution. *FEBS Lett.* **1992**, *306*, 119−124.

(16) Norris, G. E.; Anderson, B. F.; Baker, E. N. Structure of Azurin from Alcaligenes Denitrificans at 2·5 Å Resolution. *J. Mol. Biol.* **1983**, *165*, 501−521.

(17) Den Blaauwen, T.; Canters, G. W. Creation of Type-1 and Type-2 Copper Sites by Addition of Exogenous Ligands to the Pseudomonas Aeruginosa Azurin His117Gly Mutant. *J. Am. Chem. Soc.* **1993**, *115*, 1121−1129.

(18) Hammann, C.; van Pouderoyen, G.; Nar, H.; Rüth, F.-X. G.; Messerschmidt, A.; Huber, R.; den Blaauwen, T.; Canters, G. W. Crystal Structures of Modified Apo-His117Gly and Apo-His46Gly Mutants of Pseudomonas Aeruginosa Azurin. *J. Mol. Biol.* **1997**, *266*, 357−365.

(19) van Pouderoyen, G.; Andrew, C. R.; Loehr, T. M.; Sanders-Loehr, J.; Mazumdar, S.; Hill, H. A. O.; Canters, G. W. Spectroscopic and Mechanistic Studies of Type-1 and Type-2 Copper Sites in *Pseudomonas Aeruginosa* Azurin As Obtained by Addition of External Ligands to Mutant His46Gly. *Biochemistry* **1996**, *35*, 1397−1407.

(20) Berry, S. M.; Baker, M. H.; Reardon, N. J. Reduction Potential Variations in Azurin through Secondary Coordination Sphere Phenylalanine Incorporations. *J. Inorg. Biochem.* **2010**, *104*, 1071−1078.

(21) Marshall, N. M.; Garner, D. K.; Wilson, T. D.; Gao, Y.-G.; Robinson, H.; Nilges, M. J.; Lu, Y. Rationally Tuning the Reduction Potential of a Single Cupredoxin beyond the Natural Range. *Nature* **2009**, *462*, 113−116.

(22) Fitzpatrick, M. B.; Obara, Y.; Fujita, K.; Brown, D. E.; Dooley, D. M.; Kohzuma, T.; Czernuszewicz, R. S. Non-Covalent Interactions in Blue Copper Protein Probed by Met16 Mutation and Electronic and Resonance Raman Spectroscopy of Achromobacter Cycloclastes Pseudoazurin. *J. Inorg. Biochem.* **2010**, *104*, 250−260.

(23) Grossmann, J. G.; Ingledew, W. J.; Harvey, I.; Strange, R. W.; Hasnain, S. S. X-Ray Absorption Studies and Homology Modeling Define the Structural Features That Specify the Nature of the Copper Site in Rusticyanin. *Biochemistry* **1995**, *34*, 8406−8414.

(24) Hall, J. F.; Kanbi, L. D.; Harvey, I.; Murphy, L. M.; Hasnain, S. S. Modulating the Redox Potential and Acid Stability of Rusticyanin

by Site-Directed Mutagenesis of Ser86. *Biochemistry* **1998**, *37*, 11451−11458.
(25) Kanbi, L. D.; Antonyuk, S.; Hough, M. A.; Hall, J. F.; Dodd, F. E.; Hasnain, S. S. Crystal Structures of the Met148Leu and Ser86Asp Mutants of Rusticyanin from Thiobacillus Ferrooxidans: Insights into the Structural Relationship with the Cupredoxins and the Multi Copper Proteins. *J. Mol. Biol.* **2002**, *320*, 263−275.
(26) Yanagisawa, S.; Crowley, P. B.; Firbank, S. J.; Lawler, A. T.; Hunter, D. M.; McFarlane, W.; Li, C.; Kohzuma, T.; Banfield, M. J.; Dennison, C. π-Interaction Tuning of the Active Site Properties of Metalloproteins. *J. Am. Chem. Soc.* **2008**, *130*, 15420−15428.
(27) Xu, F.; Berka, R. M.; Wahleithner, J. A.; Nelson, B. A.; Shuster, J. R.; Brown, S. H.; Palmer, A. E.; Solomon, E. I. Site-Directed Mutations in Fungal Laccase: Effect on Redox Potential, Activity and pH Profile. *Biochem. J.* **1998**, *334*, 63−70.
(28) Xu, F.; Palmer, A. E.; Yaver, D. S.; Berka, R. M.; Gambetta, G. A.; Brown, S. H.; Solomon, E. I. Targeted Mutations in a Trametes Villosa Laccase: Axial Perturbations of the T1 Copper. *J. Biol. Chem.* **1999**, *274*, 12372−12375.
(29) Ledesma, G. N.; Murgida, D. H.; Ly, H. K.; Wackerbarth, H.; Ulstrup, J.; Costa-Filho, A. J.; Vila, A. J. The Met Axial Ligand Determines the Redox Potential in Cu_A Sites. *J. Am. Chem. Soc.* **2007**, *129*, 11884−11885.
(30) New, S. Y.; Marshall, N. M.; Hor, T. S. A.; Xue, F.; Lu, Y. Redox Tuning of Two Biological Copper Centers through Non-Covalent Interactions: Same Trend but Different Magnitude. *Chem. Commun.* **2012**, *48*, 4217.
(31) Leguto, A. J.; Smith, M. A.; Morgada, M. N.; Zitare, U. A.; Murgida, D. H.; Lancaster, K. M.; Vila, A. J. Dramatic Electronic Perturbations of Cu_A Centers via Subtle Geometric Changes. *J. Am. Chem. Soc.* **2019**, *141*, 1373−1381.
(32) Zitare, U. A.; Szuster, J.; Santalla, M. C.; Llases, M. E.; Morgada, M. N.; Vila, A. J.; Murgida, D. H. Fine Tuning of Functional Features of the Cu_A Site by Loop-Directed Mutagenesis. *Inorg. Chem.* **2019**, *58*, 2149−2157.
(33) Miller, A.-F. Redox Tuning over Almost 1 V in a Structurally Conserved Active Site: Lessons from Fe-Containing Superoxide Dismutase. *Acc. Chem. Res.* **2008**, *41*, 501−510.
(34) Miller, A.; Yikilmaz, E.; Vance, C.; Schwartz, A.; Xie, J.; Brunold, T. Redox Tuning over 600 MV in Superoxide Dismutase. In *Abstracts of Papers of The American Chemical Society*; Amer Chemical Soc: 1155 16th St, NW, Washington, DC 20036, USA, 2004; Vol. *227*, p U1432.
(35) Yikilmaz, E.; Porta, J.; Grove, L. E.; Vahedi-Faridi, A.; Bronshteyn, Y.; Brunold, T. C.; Borgstahl, G. E.; Miller, A.-F. How Can a Single Second Sphere Amino Acid Substitution Cause Reduction Midpoint Potential Changes of Hundreds of Millivolts? *J. Am. Chem. Soc.* **2007**, *129*, 9927−9940.
(36) Miller, A.-F.; Wang, T. A Single Outer-Sphere Mutation Stabilizes Apo-Mn Superoxide Dismutase by 35 °C and Disfavors Mn Binding. *Biochemistry* **2017**, *56*, 3787−3799.
(37) Bhagi-Damodaran, A.; Petrik, I. D.; Marshall, N. M.; Robinson, H.; Lu, Y. Systematic Tuning of Heme Redox Potentials and Its Effects on O_2 Reduction Rates in a Designed Oxidase in Myoglobin. *J. Am. Chem. Soc.* **2014**, *136*, 11882−11885.
(38) Hosseinzadeh, P.; Mirts, E. N.; Pfister, T. D.; Gao, Y.-G.; Mayne, C.; Robinson, H.; Tajkhorshid, E.; Lu, Y. Enhancing Mn(II)-Binding and Manganese Peroxidase Activity in a Designed Cytochrome c Peroxidase through Fine-Tuning Secondary-Sphere Interactions. *Biochemistry* **2016**, *55*, 1494−1502.
(39) Langen, R.; Jensen, G. M.; Jacob, U.; Stephens, P. J.; Warshel, A. Protein Control of Iron-Sulfur Cluster Redox Potentials. *J. Biol. Chem.* **1992**, *267*, 25625−25627.
(40) Chen, K.; Tilley, G. J.; Sridhar, V.; Prasad, G. S.; Stout, C. D.; Armstrong, F. A.; Burgess, B. K. Alteration of the Reduction Potential of the $[4Fe\text{-}4S]^{2+/+}$ Cluster of Azotobacter Vinelandii Ferredoxin I. *J. Biol. Chem.* **1999**, *274*, 36479−36487.
(41) Beck, B. W.; Xie, Q.; Ichiye, T. Sequence Determination of Reduction Potentials by Cysteinyl Hydrogen Bonds and Peptide Dipoles in [4Fe-4S] Ferredoxins. *Biophys. J.* **2001**, *81*, 601−613.
(42) Zuris, J. A.; Halim, D. A.; Conlan, A. R.; Abresch, E. C.; Nechushtai, R.; Paddock, M. L.; Jennings, P. A. Engineering the Redox Potential over a Wide Range within a New Class of FeS Proteins. *J. Am. Chem. Soc.* **2010**, *132*, 13120−13122.
(43) Hosseinzadeh, P.; Marshall, N. M.; Chacón, K. N.; Yu, Y.; Nilges, M. J.; New, S. Y.; Tashkov, S. A.; Blackburn, N. J.; Lu, Y. Design of a Single Protein That Spans the Entire 2-V Range of Physiological Redox Potentials. *Proc. Natl. Acad. Sci. U. S. A.* **2016**, *113*, 262−267.
(44) Mizoguchi, T. J.; Di Bilio, A. J.; Gray, H. B.; Richards, J. H. Blue to Type 2 Binding. Copper(II) and Cobalt(II) Derivatives of a Cys112Asp Mutant of Pseudomonas Aeruginosa Azurin. *J. Am. Chem. Soc.* **1992**, *114*, 10076−10078.
(45) Nilges, M. J.; Mattson, K.; Belford, R. L. Simpow6: A Software Package for the Simulation of ESR Powder-Type Spectra. *ESR Spectrosc. Membr. Biophys.* **2007**, *27*, 261−281.
(46) Chang, H. R.; Diril, H.; Nilges, M. J.; Zhang, X.; Potenza, J. A.; Schugar, H. J.; Hendrickson, D. N.; Isied, S. S. An Unusually Stable Manganese(II) Manganese(III) Complex with Novel EPR Spectra: Synthesis, Structure, Magnetism, and EPR Analysis. *J. Am. Chem. Soc.* **1988**, *110*, 625−627.
(47) Jeuken, L. J.; Armstrong, F. A. Electrochemical Origin of Hysteresis in the Electron-Transfer Reactions of Adsorbed Proteins: Contrasting Behavior of the "Blue" Copper Protein, Azurin, Adsorbed on Pyrolytic Graphite and Modified Gold Electrodes. *J. Phys. Chem. B* **2001**, *105*, 5271−5282.
(48) Winter, G. Xia2: An Expert System for Macromolecular Crystallography Data Reduction. *J. Appl. Crystallogr.* **2010**, *43*, 186−190.
(49) Winter, G.; Waterman, D. G.; Parkhurst, J. M.; Brewster, A. S.; Gildea, R. J.; Gerstel, M.; Fuentes-Montero, L.; Vollmar, M.; Michels-Clark, T.; Young, I. D.; Sauter, N. K.; Evans, G. DIALS: Implementation and Evaluation of a New Integration Package. *Acta Crystallogr., Sect. D: Struct. Biol.* **2018**, *74*, 85−97.
(50) Evans, P. R.; Murshudov, G. N. How Good Are My Data and What Is the Resolution? *Acta Crystallogr., Sect. D: Biol. Crystallogr.* **2013**, *69*, 1204−1214.
(51) Winn, M. D.; Ballard, C. C.; Cowtan, K. D.; Dodson, E. J.; Emsley, P.; Evans, P. R.; Keegan, R. M.; Krissinel, E. B.; Leslie, A. G.; McCoy, A.; et al. Overview of the CCP4 Suite and Current Developments. *Acta Crystallogr., Sect. D: Biol. Crystallogr.* **2011**, *67*, 235−242.
(52) Potterton, L.; Agirre, J.; Ballard, C.; Cowtan, K.; Dodson, E.; Evans, P. R.; Jenkins, H. T.; Keegan, R.; Krissinel, E.; Stevenson, K.; et al. CCP4i2: The New Graphical User Interface to the CCP4 Program Suite. *Acta Crystallogr., Sect. D: Struct. Biol.* **2018**, *74*, 68−84.
(53) Adams, P. D.; Afonine, P. V.; Bunkóczi, G.; Chen, V. B.; Davis, I. W.; Echols, N.; Headd, J. J.; Hung, L.-W.; Kapral, G. J.; Grosse-Kunstleve, R. W.; et al. PHENIX: A Comprehensive Python-Based System for Macromolecular Structure Solution. *Acta Crystallogr., Sect. D: Biol. Crystallogr.* **2010**, *66*, 213−221.
(54) McCoy, A. J.; Grosse-Kunstleve, R. W.; Adams, P. D.; Winn, M. D.; Storoni, L. C.; Read, R. J. Phaser Crystallographic Software. *J. Appl. Crystallogr.* **2007**, *40*, 658−674.
(55) Emsley, P.; Cowtan, K.; Lohkamp, B.; Scott, W. G. Features and Development of Coot. *Acta Crystallogr., Sect. D: Biol. Crystallogr.* **2010**, *66*, 486−501.
(56) Chen, V. B.; Arendall, W. B.; Headd, J. J.; Keedy, D. A.; Immormino, R. M.; Kapral, G. J.; Murray, L. W.; Richardson, J. S.; Richardson, D. C. MolProbity: All-Atom Structure Validation for Macromolecular Crystallography. *Acta Crystallogr., Sect. D: Biol. Crystallogr.* **2010**, *66*, 12−21.
(57) Laskowski, R. A.; MacArthur, M. W.; Moss, D. S.; Thornton, J. M. PROCHECK: A Program to Check the Stereochemical Quality of Protein Structures. *J. Appl. Crystallogr.* **1993**, *26*, 283−291.

https://doi.org/10.1021/acs.inorgchem.3c01365
Inorg. Chem. 2023, 62, 11618−11625

(58) Pettersen, E. F.; Goddard, T. D.; Huang, C. C.; Meng, E. C.; Couch, G. S.; Croll, T. I.; Morris, J. H.; Ferrin, T. E. UCSF ChimeraX: Structure Visualization for Researchers, Educators, and Developers. *Protein Sci.* **2021**, *30*, 70−82.
(59) Solomon, E. I.; Hare, J. W.; Dooley, D. M.; Dawson, J. H.; Stephens, P. J.; Gray, H. B. Spectroscopic Studies of Stellacyanin, Plastocyanin, and Azurin. Electronic Structure of the Blue Copper Sites. *J. Am. Chem. Soc.* **1980**, *102*, 168−178.
(60) Gray, H. B.; Malmström, B. G. On the Relationship between Protein-Forced Ligand Fields and the Properties of Blue Copper Centers. *Comments Inorg. Chem.* **1983**, *2*, 203−209.
(61) Solomon, E. I.; Heppner, D. E.; Johnston, E. M.; Ginsbach, J. W.; Cirera, J.; Qayyum, M.; Kieber-Emmons, M. T.; Kjaergaard, C. H.; Hadt, R. G.; Tian, L. Copper Active Sites in Biology. *Chem. Rev.* **2014**, *114*, 3659−3853.
(62) Nar, H.; Huber, R.; Messerschmidt, A.; Filippou, A. C.; Barth, M.; Jaquinod, M.; Kamp, M.; Canters, G. W. Characterization and Crystal Structure of Zinc Azurin, a by-Product of Heterologous Expression in Escherichia Coli of Pseudomonas Aeruginosa Copper Azurin. *Eur. J. Biochem.* **1992**, *205*, 1123−1129.
(63) Hoitink, C.; Canters, G. W. The Importance of Asn47 for Structure and Reactivity of Azurin from Alcaligenes Denitrificans as Studied by Site-Directed Mutagenesis and Spectroscopy. *J. Biol. Chem.* **1992**, *267*, 13836−13842.
(64) Wimley, W. C.; White, S. H. Experimentally Determined Hydrophobicity Scale for Proteins at Membrane Interfaces. *Nat. Struct. Biol.* **1996**, *3*, 842−848.
(65) Wimley, W. C.; Creamer, T. P.; White, S. H. Solvation Energies of Amino Acid Side Chains and Backbone in a Family of Host- Guest Pentapeptides. *Biochemistry* **1996**, *35*, 5109−5124.
(66) Tsai, L.-C.; Bonander, N.; Harata, K.; Karlsson, G.; Vänngå, T. Mutant Met121Ala of Pseudomonas Aeruginosa Azurin and Its Azide Derivative: Crystal Structures and Spectral Properties. *Acta Crystallogr., Sect. D: Biol. Crystallogr.* **1996**, *52*, 950−958.
(67) Lancaster, K. M.; George, S. D.; Yokoyama, K.; Richards, J. H.; Gray, H. B. Type-Zero Copper Proteins. *Nat. Chem.* **2009**, *1*, 711−715.
(68) Lancaster, K. M.; Yokoyama, K.; Richards, J. H.; Winkler, J. R.; Gray, H. B. High-Potential C112D/M121X (X= M, E, H, L) Pseudomonas Aeruginosa Azurins. *Inorg. Chem.* **2009**, *48*, 1278−1280.
(69) Tian, S.; Liu, J.; Cowley, R. E.; Hosseinzadeh, P.; Marshall, N. M.; Yu, Y.; Robinson, H.; Nilges, M. J.; Blackburn, N. J.; Solomon, E. I.; Lu, Y. Reversible S-Nitrosylation in an Engineered Azurin. *Nat. Chem.* **2016**, *8*, 670−677.
(70) Hadt, R. G.; Sun, N.; Marshall, N. M.; Hodgson, K. O.; Hedman, B.; Lu, Y.; Solomon, E. I. Spectroscopic and DFT Studies of Second-Sphere Variants of the Type 1 Copper Site in Azurin: Covalent and Nonlocal Electrostatic Contributions to Reduction Potentials. *J. Am. Chem. Soc.* **2012**, *134*, 16701−16716.

https://doi.org/10.1021/acs.inorgchem.3c01365
Inorg. Chem. 2023, 62, 11618−11625